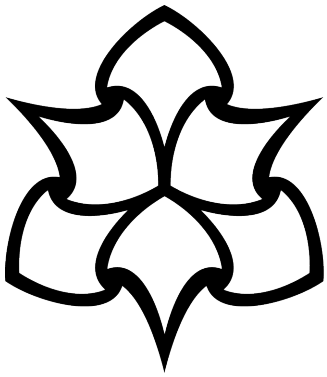

Synthesis, characterisation and electrochemistry of eight Fe coordination compounds containing substituted 2-(1-(4-R-phenyl-1H-1,2,3-triazol-4-yl)pyridine ligands, R = CH_3, OCH_3, COOH, F, Cl, CN, H and CF_3.

J. Conradie[1*], M.M. Conradie[1], Z. Mtshali[1], D. van der Westhuizen[1], K.M. Tawfiq[2,3], M.J. Al-Jeboori[3], S.J. Coles,[4] C. Wilson[5] and J.H. Potgieter[2,6*]

1. Department of Chemistry, University of the Free State, P.O. Box 339, Bloemfontein, 9300, South Africa

2. Division of Chemistry and Environmental Science, Manchester Metropolitan University, Manchester, M1 5GD, UK

3. Department of Chemistry, College of Education for Pure Science (Ibn Al-Haitham), University of Baghdad, Baghdad, Iraq

4. EPSRC National Crystallography Service, Chemistry, University of Southampton, Southampton, SO17 1BJ, England

5. School of Chemistry, University of Glasgow, Joseph Black Building. University Avenue, Glasgow, G12 8QQ, Scotland

6. School of Chemical and Metallurgical Engineering, University of the Witwatersrand, Private Bag X3, Wits, 2050, South Africa

*Contact author details:

Name: Jeanet Conradie

Tel: +27-51-4012194

Fax: +27-51-4017295

e-mail: conradj@ufs.ac.za

Abstract

Eight different Dichloro(bis{2-[1-(4-R-phenyl)-1H-1,2,3-triazol-4-yl-κN^3]pyridine-κN})iron(II) compounds, **2** – **9**, have been synthesised and characterised, where group R = CH_3 (L^2), OCH_3 (L^3), COOH (L^4), F (L^5), Cl (L^6), CN (L^7), H (L^8) and CF_3 (L^9). The single crystal X-ray structure was determined for the L^3 which was complemented with Density Functional Theory calculations for all complexes. The structure exhibits a distorted octahedral geometry, with the two triazole ligands coordinated to the iron centre positioned in the equatorial plane and the two chloro atoms in the axial positions. The values of the $Fe^{II/III}$ redox couple, observed at *ca.* –0.3 V *versus* Fc/Fc^+ for

complexes **2** – **9**, varied over a very small potential range of 0.05 V. The observation that the different R substituents have virtually no effect on the values of the $Fe^{II/III}$ redox couple for all eight complexes **2** – **9**, is explained by the character of the highest molecular orbitals of complexes **2** – **9**, which do not show any communication of electron density between the various ligands and the metal Fe. However, the HOMOs of the free ligands L^2 – L^9, display extended π-character over the entire ligand, explaining the sensitivity of the ^{1}H NMR C-H-triazole peak, which is dependent on the electron donating/withdrawing power of the R substituent attached to the 2-[1-(4-R-phenyl)-1H-1,2,3-triazol-4-yl]pyridine ligands.

Keywords

(1,2,3-triazol-4-yl)pyridine; redox potential; iron; DFT

TOC graphics and text

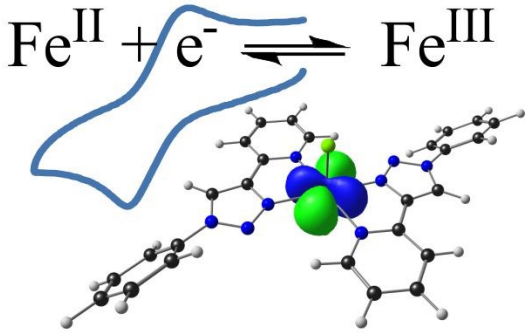

$Fe^{II/III}$ redox couple of Fe-(1,2,3-triazol-4-yl)pyridine complexes, observed at *ca.* –0.3 V *vs*. the $Fe^{II/III}$ redox couple of ferrocene.

Highlights

Fe-(1,2,3-triazol-4-yl)pyridine complexes demonstrate intermolecular H bonding in the solid state

Fe-(1,2,3-triazol-4-yl)pyridine complexes display π…π stacking in the solid state

$Fe^{II/III}$ redox couple is observed at *ca.* –0.3 V *vs*. the $Fe^{II/III}$ redox couple of ferrocene.

DFT calculations show that Fe-(1,2,3-triazol-4-yl)pyridine is high spin

1 Introduction

This study makes use of cycloaddition as synthetic method, an important strategy for constructing stereochemically complex heterocyclic compounds, which is a vital area of organic chemistry. Asymmetric [1,2] cycloaddition reactions, via chiral catalysts complexed to various metals, have recently been developed as new methods for designing technology specific complex heterocyclic compounds. Different five-membered ring systems can be very effectively synthesised via cycloaddition, starting with 2-atom or 3-atom precursors [1,2]. There are a variety of cycloaddition methods, e.g. also including 1,3-dipolar cycloadditions, which are very efficient in synthesising medicinal molecules and complex natural products [3]. A 1,2,3-triazole structure contains three adjacent nitrogen atoms with three available substitution sites and is a basic aromatic heterocyclic compound [4]. 1,2,3-Triazole is a useful building block [5] when constructing more complex chemical compounds for specific applications, e.g. for medical applications (antimicrobial) [6] or chemical industrial use [7]. In this work a series eight of 1,2,3-triazole chromophores [10] were synthesized though the copper(I)-catalysed azide alkyne cycloaddition (CuAAC) "click" reaction [8] and then coordinated to iron(II) to prepare a variety of eight iron complexes 2 – 9 (Figure 1), with potential application as photo-sensitizers for potential use in DSSCs. The first row transition metal Fe was chosen due its general availability and cost effectiveness as alternative to ruthenium metal [9], which is currently popular in dye solar cell research. For future evaluation of the compounds to be used as dyes in DSSCs, a detailed knowledge of their structure and properties is essential. The properties and characterisation of the chromophore ligands and their iron complexes, schematically shown in Figure 1, are presented and discussed, including the crystal structure for **3**, as well as computational chemistry and electrochemistry results.

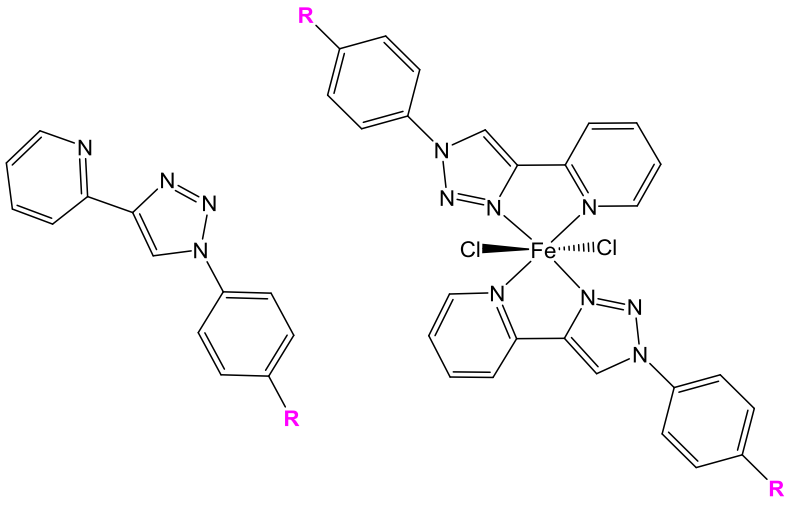

Figure 1: Structure of the 1,2,3-triazole free ligands (L^2-L^9) and their respective iron complexes (2 – 9), where substituent R = CH_3 (L^2) [20], OCH_3 (L^3), COOH (L^4), F (L^5), Cl (L^6), CN (L^7), H (L^8) and CF_3 (L^9).

2 Methods and Materials

2.1 Synthesis of (1,2,3-triazol-4-yl)pyridine ligands

The (1,2,3-triazol-4-yl)pyridine free ligands ($L^2 – L^9$) were synthesised and characterised, as has been described previously for $L^2 – L^9$ [10], L^2 [11], L^3 [12][13][14], L^6 [15], L^8 [16][17][18], see the reaction scheme in Scheme 1.

2.2 Synthesis of (1,2,3-triazol-4-yl)pyridine ligand iron(II) complexes

The general approach for the synthesis of all the iron(II) complexes was carried out according to a standard literature procedure, with small modifications as required [17]. For iron(II) complexes **2, 3**, **5** – **9**, an appropriate amount of ferrous chloride (1 equiv. ca 3 mmol) was dissolved in methanol (10 ml) and added dropwise to a solution of the ligand (2 equiv. ca 6 mmol) in CH_2Cl_2 (10ml). The mixture was stirred at room temperature (RT) for 8 – 10 h, the solvent was removed under vacuum, the solid mass recovered and washed with several volumes of cold methanol and diethyl ether. Due to the poor solubility of the carboxylic group containing ligand L^4, the synthesis was changed as follow for complex **4**: ferrous chloride (1equiv. ca 3 mmol) was dissolved in methanol (10 ml) and added dropwise to a solution of the ligand (2equiv. ca 6 mmol) in DMSO (10ml). The reaction mixture was stirred at RT for 10 min and then allowed to reflux for 24h. The solvent was reduced in volume by a half under vacuum distillation and crushed ice was added to the solution. The precipitate was filtered before being washed twice with cold methanol and then diethyl ether. A similar poor solubility was reported for ligand btp, which is 2,6-bis(1-(4-(carboxy)benzyl)-1,2,3-triazol-4-yl)pyridine [19]. These methods proved very satisfactory and provided good yields, ranging from 73-83% (see below for exact yields). The reaction for **2, 3**, **5** – **9** is represented in Scheme 2. The characterisation data of the paramagnetic Fe(II) complexes are given below.

2.2.1 Characterisation of Dichloro(bis{2-[1-(4-methylphenyl)-1H-1,2,3-triazol-4-yl-κN^3]pyridine-κN})iron(II), Complex **2** (containing L^2 with R = CH_3) [20]

Yield 83%, mp. 308-310 °C. IR: $\bar{\nu}$ (cm^{-1}): 3063, 3047, 3025, 1605, 1595, 1571, 1522, 1473, 1448, 1267, 1258, 1063, 1054, 1015, 1004, 886, 815, 786, 553. UV-Vis (DMSO) λ_{max}: The Fe(II) complex showed absorption bands at 259 nm, ε_{max} = 65500 $dm^3mol^{-1}cm^{-1}$, 287 nm, ε_{max} = 52000 $dm^3mol^{-1}cm^{-1}$, 326 nm, ε_{max} = 4783 $dm^3mol^{-1}cm^{-1}$, 908 nm, ε_{max} = 85 $dm^3mol^{-1}cm^{-1}$. HRMS TOF (ESI+) (water:

acetonitrile = 1:3) with the highest molecular weight ion peak matching, was observed at m/z = 563.1135 (80%) and is attributed to $[[Fe(L^2)_2Cl_2] - Cl]^+$. The calculated value for $[(C_{28}H_{24}N_8FeCl)]^+$ is 563.1162. μ_{eff} = 5.26 B.M. Elemental Anal. Calc. for $C_{28}H_{24}N_8Cl_2Fe$: C, 56.1; H, 4.0; N 18.7. Found: C, 56.0; H, 4.1; N 18.8%.

2.2.2 Characterisation of Dichloro(bis{2-[1-(4-methoxyphenyl)-1H-1,2,3-triazol-4-yl-κN^3]pyridine-κN})iron(II), Complex **3** (containing L^3 with R = OCH_3)

Yield 83%, mp. 308-310 °C. IR: $\bar{\nu}$ (cm^{-1}): 3054, 3032, 3012, 2965, 2865, 2838, 1606, 1571, 1518, 1469, 1448, 1289, 1261, 1182, 1065, 1055, 1017, 1002, 979, 858, 825, 786, 719. UV-Vis (DMSO) λ_{max}: The Fe(II) complex showed absorption bands at 256nm, ε_{max} = 35500 $dm^3mol^{-1}cm^{-1}$, 291 nm, ε_{max} = 17500 $dm^3mol^{-1}cm^{-1}$, 333 nm, ε_{max} = 3810 $dm^3mol^{-1}cm^{-1}$, 922nm, ε_{max} = 65 $dm^3mol^{-1}cm^{-1}$. HRMS TOF (ESI+) (water: acetonitrile = 1:3) with the highest molecular weight ion peak matching, was observed at m/z = 595.1055 (88%) and is attributed to $[[Fe(L^3)_2Cl_2] - Cl]^+$. The calculated value for $[(C_{28}H_{24}ClFeN_8O_2)]^+$ is 595.1060. μ_{eff} = 5.07 B.M. Elemental Anal. Calc. for $C_{28}H_{24}N_8Cl_2O_2Fe$: C, 53.3; H, 3.8; N 17.8. Found: C, 53.0; H, 3.71; N 17.5%.

2.2.3 Characterisation of Dichloro(bis{4-[4-(pyridin-2-yl-κN)-1H-1,2,3-triazol-1-yl-κN^3]benzoic acid})iron(II), Complex **4** (containing L^4 with R = COOH)

Yield 73%, mp. 348-350 °C. IR: $\bar{\nu}$ (cm^{-1}): 3085, 1724, 1604, 1589, 1514, 1471, 1450, 1406, 1372, 1254, 1173, 1104, 1055, 1018, 1004, 978, 857, 774. UV-Vis (DMSO) λ_{max}: The Fe (II) complex showed absorption bands at 258 nm, ε_{max} = 181600 $dm^3mol^{-1}cm^{-1}$, 291nm, ε_{max} = 86500 $dm^3mol^{-1}cm^{-1}$, 332 nm, ε_{max} = 7053 $dm^3mol^{-1}cm^{-1}$. HRMS TOF (MALDI) with the highest molecular weight ion peak matching, was observed at m/z = 623.1 (100%) and is related to $[[Fe(L^4)_2Cl_2] - Cl]^+$. The calculated value for $[C_{28}H_{20}N_8FeO_4Cl]^+$ is 623.100. μ_{eff} = 5.1 B.M. Elemental Anal. Calc. for $C_{28}H_{20}N_8Cl_2O_4Fe$: C, 51.0; H, 3.1; N 17.0. Found: C, 51.3; H, 2.9; N 16.8%.

2.2.4 Characterisation of Dichloro(bis{2-[1-(4-fluorophenyl)-1H-1,2,3-triazol-4-κN^3]pyridine-κN})iron(II), Complex **5** (containing L^5 with R = F)

Yield 75%, mp. 258-260 °C. IR: $\bar{\nu}$ (cm^{-1}): 3065, 3041, 3026, 1605, 1578, 1515, 1472, 1453, 1412, 1333, 1239, 1258, 1159, 1061, 1015, 1005, 979, 837, 788, 718. UV-Vis (DMSO) λ_{max}: The Fe(II) complex showed absorption bands at 257 nm, ε_{max} = 69630 $dm^3mol^{-1}cm^{-1}$, 286nm, ε_{max} = 3111 $dm^3mol^{-1}cm^{-1}$, 329 nm, ε_{max} = 3380 $dm^3mol^{-1}cm^{-1}$. HRMS TOF (MALDI) with the highest molecular weight ion peak matching, was observed at *m/z* = 571.0635 (35%) and is assigned to $[[Fe(L^5)_2Cl_2] - Cl]^+$. The calculated value for $[C_{26}H_{18}F_2N_8FeCl]^+$ is 571.0660. μ_{eff} = 4.87 B.M. Elemental Anal. Calc. for $C_{26}H_{18}N_8Cl_2F_2Fe$: C, 51.4; H, 3.0; N 18.5. Found: C, 51.6; H, 2.8; N 18.2%.

2.2.5 Characterisation of Dichloro(bis{2-[1-(4-chlorophenyl)-1H-1,2,3-triazol-4-yl-κN^3]pyridine-κN})iron(II), Complex **6** (containing L^6 with R = Cl)

Yield 79%, mp. 258-260 °C. IR: $\bar{\nu}$ (cm^{-1}): 3051, 3023, 3005, 1606, 1591, 1570, 1502, 1472, 1448, 1405, 1267, 1257, 1151, 1134, 1095, 1061, 1052, 1013, 1003, 977, 860, 825, 808, 789, 711. UV-Vis (DMSO) λ_{max}: The Fe(II) complex showed absorption bands at 258 nm, ε_{max} = 58571 dm^{3}mol^{-1}cm^{-1}, 287 nm, ε_{max} = 47143 dm^{3}mol^{-1}cm^{-1}, 332 nm, ε_{max} = 4060 dm^{3}mol^{-1}cm^{-1}, 386 nm, ε_{max} = 2020 dm^{3}mol^{-1}cm^{-1}. HRMS (ESI+) (water: acetonitrile = 1:3) with the highest molecular weight ion peak matching, was observed at *m/z* = 603.0050 (75%) and is related to $[[Fe(L^6)_2Cl_2] - Cl]^+$. The calculated value for $[C_{26}H_{18}N_8FeCl_3]^+$ is 603.0069. μ_{eff} = 5.10 B.M. Elemental Anal. Calc. for $C_{26}H_{18}N_8Cl_4Fe$: C, 48.8; H, 2.8; N 17.5. Found: C, 49.0; H, 3.0; N 17.3%.

2.2.6 Characterisation of Dichloro(bis{4-[4-(pyridin-2-yl-κN)-1H-1,2,3-triazol-1-yl-κN^3]benzonitrile})iron(II), Complex **7** (containing L^7 with R = CN)

Yield 83%, mp. 308-310 °C. IR: $\bar{\nu}$ (cm^{-1}): 3071, 3057, 3025, 3012, 2233, 1604, 1591, 1572, 1514, 1471, 1451, 1410, 1287, 1258, 1259, 1140, 1061, 1052, 1016, 1006,977, 846, 787, 717. UV-Vis (DMSO) λ_{max}: The Fe(II) complex showed absorption bands at 256 nm, ε_{max} = 138750 dm^{3}mol^{-1}cm^{-1}, 289 nm, ε_{max} = 56250 dm^{3}mol^{-1}cm^{-1}, 950 nm, ε_{max} = 45 dm^{3}mol^{-1}cm^{-1}. HRMS TOF (ESI+) (water: acetonitrile = 1:3) with the highest molecular weight ion peak matching, was observed at m/z = 585.0738 (70%) and is assigned to $[[Fe(L^7)_2Cl_2] - Cl]^+$. The calculated value for $[C_{28}H_{18}N_{10}ClFe]^+$ is 585.0754. μ_{eff} = 4.26 B.M. Elemental Anal. Calc. for $C_{28}H_{18}N_{10}Cl_2Fe$: C, 54.1; H, 2.9; N 22.6. Found: C, 54.4; H, 3.1; N 22.6%.

2.2.7 Characterisation of Dichloro{bis[2-(1-phenyl-1H-1,2,3-triazol-4-yl-κN^3]pyridine-κN]}iron(II), Complex **8** (containing L^8 with R = H)

Yield 81%, mp. 336-338 °C. IR: $\bar{\nu}$ (cm^{-1}): 3064, 3053, 3026, 3009, 1606, 1594, 1575, 1504, 1471, 1444, 1267, 1259, 1063, 1054, 1016, 1004, 977, 913, 861, 815, 785, 756, 725, 686. UV-Vis (DMSO) λ_{max}: The Fe(II) complex showed absorption bands at 258 nm, ε_{max} = 62593 dm^{3}mol^{-1}cm^{-1}, 286 nm, ε_{max} = 32963 dm^{3}mol^{-1}cm^{-1}, 333nm, ε_{max} = 52917 dm^{3}mol^{-1}cm^{-1}, 522nm, ε_{max} = 190 dm^{3}mol^{-1}cm^{-1}, 756 nm, ε_{max} = 885 dm^{3}mol^{-1}cm^{-1}. HRMS TOF (ESI+) (water: acetonitrile = 1:3) with the highest molecular weight ion peak matching, was observed at *m/z* = 535.0835 (60%) and is related to $[[Fe(L^8)_2Cl_2] - Cl]^+$. The calculated value for $[C_{26}H_{20}N_8ClFe]^+$ is 535.0849. μ_{eff} = 4.66 B.M. Elemental Anal. Calc. for $C_{26}H_{20}N_8Cl_2Fe$: C, 54.7; H, 3.5; N 19.6. Found: C, 54.5; H, 3.8; N 19.6%.

2.2.8 Characterisation of Dichloro[bis(2-{1-[4-(trifluoromethyl)phenyl]-1H-1,2,3-triazol-4-κN^3]pyridine-κN)]iron(II), Complex **9** (containing L^9 with R = CF_3)

Yield 83%, mp. 274-276°C. IR: $\bar{\nu}$ (cm^{-1}): 3063, 3047, 3025, 1605, 1595, 1571, 1522, 1473, 1448, 1267, 1258, 1060, 1049, 1015, 1005, 886, 815, 786. UV-Vis (DMSO) λ_{max}: The Fe (II) complex showed absorption bands at 258 nm, ε_{max} = 58947 dm^3 $mol^{-1}cm^{-1}$, 288nm, ε_{max} = 48947 $dm^3mol^{-1}cm^{-1}$, 326 nm, ε_{max} = 4511 $dm^3mol^{-1}cm^{-1}$, 566 nm, ε_{max} = 461 $dm^3mol^{-1}cm^{-1}$, 590 nm, ε_{max} = 453 $dm^3mol^{-1}cm^{-1}$ respectively. HRMS TOF (MALDI) with the highest molecular weight ion peak matching, was observed at m/z = 671.1 (100%) and is attributed to $[[Fe(L^9)_2Cl_2] - Cl]^+$. The calculated value for $[C_{28}H_{18}ClF_6N_8Fe]^+$ is 671.100. μ_{eff} = 4.72 B.M. Elemental Anal. Calc. for $C_{28}H_{18}N_8Cl_2F_6Fe$: C, 47.6; H, 2.6; N 15.9. Found: C, 47.7; H, 2.3; N 15.7%.

2.3 Instrumental conditions and measurement parameters

Infrared (ATR-FTIR IR) spectra were recorded using a smart diamond ATR attachment on a Thermo-Nicolet FT-IR Spectrometer (AVATAR 320), over a range of 4000 to 400 cm^{-1}. Mass spectra were performed at EPSRC Mass Spectrometry Service Centre, University of Wales, Swansea and University of Sheffield. The instrument used was the 'WATERS LCT premier', the solvent was water/acetonitrile (1:3), while the ionisation was electrospray (ESI+ and ES-). Thermofisher LTQ Orbitrap XL, used to analyse volatile molecules in the mass range of m/z 50–2000 or m/z 200–4000 Daltons. UV-Vis spectra were obtained on a PerkinElmer Lambda 40 UV/Vis spectrometer. Each sample ($1x10^{-5}$ M) was analysed using a constant blank of acetonitrile. A pair of identical quartz cells with a path length of 1cm were used to reduce the interference from the cells themselves. Further spectra was obtained for specific complexes at a concentration of $1x10^{-3}$ M when some absorbance was visible albeit at a very low level. The absorbance was measured over a wavelength range of 250 nm to 900 nm.

2.4 Magnetic susceptibility

Magnetic susceptibility of the complexes was measured with a Gouy magnetic susceptibility balance. The gram magnetic susceptibility for a substance is calculated from:

$$\chi_g = (C_{bal})\ (l)\ (R - R_o) / (10^9)\ (m)$$

Where l = height of sample in the tube in units of centimeters, m = mass of the sample in units of grams, R = reading for tube plus sample, R_o = reading for the empty tube and C_{bal} = balance calibration

constant = 1.0. The molar magnetic susceptibility is then calculated from the gram magnetic susceptibility using the following equation.

$\chi_m = (\chi_g)$ **(molar mass)**

The effective magnetic moment for a particular substance is calculated from the molar magnetic susceptibility [21] using the following equation (T represents the Kelvin temperature (294 K)):

$\mu_{eff} = 2.83\ [(\chi_m)\ (T)]^{1/2}$

2.5 X-ray diffraction

The crystal of complex **3** $[Fe(L^3)_2Cl_2]$ with ligand $\mathbf{L^3}$ (where R = OCH_3) suitable for a single crystal diffraction data collection, was obtained by slow evaporation in a hot mixture of a DMSO : acetonitrile = 1 : 9 solution, under ambient conditions. Single crystal X-ray diffraction data were collected using a Rigaku Saturn 724+ area detector, mounted at the window of an FR-E+ rotating anode generator, with wavelength Mo Kα, λ = 0.71075Å [22]. The crystals were mounted on a Mitegen loop and data was collected at 100K, under nitrogen flow from an Oxford Cryosystems Cobra device. The structures were solved by direct methods, using the program SHELXS-97 within OLEX2 [23]. All refinements on F_o^2 by full-matrix least squares refinement, were performed using the SHELXL-97 program package [24] within the OLEX2 software. All non-hydrogen atoms were refined with anisotropic atomic displacement parameters, and hydrogen atoms were added at calculated positions and included as part of a riding model with C-H (aromatic) 0.95Å $U_{ISO} = 1.2U_{eq}$ (C); and C-H (methyl) 0.98Å $U_{ISO} = 1.5U_{eq}$ (C) [57]. A perspective drawing of the molecular structure of complex $[Fe(L^3)_2Cl_2]$, showing the atom numbering scheme, is shown in Figure 6. Crystallographic data is presented in Table 1, with selected bond lengths (Å) and bond angles (°) listed in Table 2. Additional crystallographic data are available free of charge from the Cambridge Crystallographic Data Centre (Deposition number CCDC 1585946).

2.6 Cyclic Voltammetry

Cyclic voltammetry measurements [25] were performed on 0.05 mmol dm^{-3} or saturated compound solutions, in dry acetonitrile/DMSO solution (Aldrich, Biotech grade 99.93+% purity, anhydrous, kept under purified argon), under a blanket of purified argon at 25 °C, utilizing a BAS 100B/W electrochemical analyzer. Due to the poor solubility of the compound in acetonitrile, each of the eight complexes was first dissolved in 0.5 ml DMSO, after which 1.5 ml acetonitrile was added. The supporting electrolyte was 0.1 mol dm^{-3} tetra-*n*-butylammonium hexafluorophosphate,

($^{n}Bu_4N$)(PF_6) (Fluka electrochemical grade). A three-electrode cell, with a glassy carbon (surface area 7.07 x 10^{-6} m^2) working electrode, Pt auxiliary electrode and a Ag/Ag^+ (0.010 mol dm^{-3} $AgNO_3$ in CH_3CN) reference electrode [26], mounted on a Luggin capillary, was used [27,28]. All temperatures were kept constant, within 0.5 °C. Successive experiments under the same experimental conditions showed that all reduction and formal reduction potentials were reproducible within 0.005 V. All cited potentials were referenced against the Fc/Fc^+ couple, as suggested by IUPAC [29]. Ferrocene exhibited a formal reduction potential of $E°' = 0.072$ V *vs.* Ag/Ag^+, a peak separation of $\Delta E_p = E_{pa} - E_{pc} = 0.070$ V, as well as a ratio $i_{pc}/i_{pa} = 0.99$ under our experimental conditions. E_{pa} (E_{pc}) = anodic (cathodic) peak potential, and i_{pa} (i_{pc}) = anodic (cathodic) peak current. $E°'$ (Fc/Fc^+) = 0.400 V *vs.* NHE [30], and SCE = 0.244 V *vs.* NHE.

2.7 Theoretical approach

Density functional theory (DFT) calculations were performed via the B3LYP functional, as implemented in the Gaussian 09 package [31], using the triple-ζ basis set 6-311G(d,p). The ligands L^2 - L^8, as well as the complex $[Fe(L^8)_2Cl_2]$, with R = H on ligand L^8, were optimized. The possible spin states of $[Fe(L^8)_2Cl_2]$ (S = 0, 1 or 2) and the cation $[Fe(L^8)_2Cl_2]^+$ (S = ½, 3/2 or 5/2) were optimized to determine the ground state of the Fe(II) complexes of this study. Natural bonding orbital (NBO) calculations [32-35] were performed on the optimised structure of ligand L^8 via the NBO 3.1 module [36] in Gaussian 09, at the same level of theory.

3 Results and discussion

The (1,2,3-triazol-4-yl)pyridine ligands (L^2 – L^9) chosen for this study, contain both electron donating (R= CH_3, OCH_3) as well as electron withdrawing groups (R = F, Cl, CN, CF_3, COOH).

3.1 Properties of (1,2,3-triazol-4-yl)pyridine free ligands L^2 – L^9

The synthesis of the (1,2,3-triazol-4-yl)pyridine free ligands (L^2 – L^9) were undertaken, using the copper(I)-catalysed azide alkyne cycloaddition (CuAAC) “click” reaction [1,2], which involves the generation of a five membered triazole ring between an aryl azide and an aryl alkene as shown in Scheme 1.

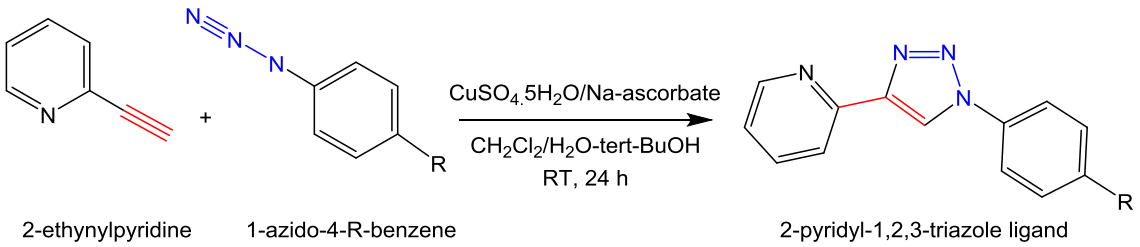

Scheme 1. Preparation route for the 2-pyridyl-[1,2,3]-triazole free ligands (L^2-L^9) from an azide and alkyne by the Cu(I) catalyzed "click" reaction where substituent R = CH_3 (L^2), OCH_3 (L^3), COOH (L^4), F (L^5), Cl (L^6), CN (L^7), H (L^8) and CF_3 (L^9).

The ^{1}H- and ^{13}C-NMR spectra for each ligand L^2 – L^9 were assigned in comparison with spectra of previously reported triazoles [11,37], and supported by 2-dimensional spectra (^{1}H–^{1}H COSY and ^{13}C–^{1}H HMQC), to confirm the proposed assignments. The chemical shift (δ) of the ^{1}H- (C-H) and ^{13}C-NMR (=CH) of the triazole moiety have been tabulated in Table S1, for ligands L^2 to L^9. The effect of the electron withdrawing substituents on the phenyl ring, manifested itself in shifts of the C-H-triazole peak of the ^{1}*H*-1,2,3-triazole system, which was observed in the range between 8.54-9.46 ppm in the ^{1}H-NMR spectra, and between 119.69-120.48 ppm in the ^{13}C-NMR spectra of ligands L^2 to L^9. The good communication between the different substituents R on the phenyl group and the rest of the ligand, results in a linear trend between the shift of the δ(C-H) triazole peak of the ^{1}*H*-1,2,3-triazole system and the para Hammett constant of the R group, see Figure 2.

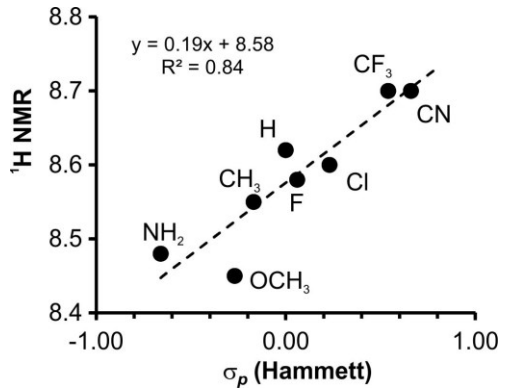

Figure 2. Relationship between the δ(C-H) triazole peak of the ^{1}*H*-1,2,3-triazole system and the para Hammett constant of the R group of the 2-pyridyl-1,2,3-triazole ligands L^2- L^9. R group is shown on the graph. Data is given in Table S1. Data (not shown) of ligand with substituent R = COOH (L^4) did not fit the trend.

The calculated density functional theory (DFT) optimised geometries of ligands L^2 to L^9, showed that the lowest energy geometry of each ligand has the NH of the triazol ring *syn* to the pyridine nitrogen, in agreement with experimental crystal structures of (1,2,3-triazol-4-yl)pyridine ligands

[38]. This preferred orientation can be explained by the stabilisation interaction between the lone pair on $N_{triazol}$, LP(N), and the antibonding orbital of $(C\text{-}H)_{pyridine}$, BD*(C-H). For ligand 8 (with R = H on L^{8}), for example, the lone pair LP(N) of the natural bond orbital (NBO) occupation 1.928 e^{-}, donated electron density to the empty antibonding orbital BD*(C-H), with occupation 0.014 e^{-}. The NBO calculation of ligand 7 detected this interaction with a second order perturbation energy of 0.5 $kJ \cdot mol^{-1}$; see Figure 3 for a visualisation of this interaction.

Although all crystal structures of (1,2,3-triazol-4-yl)pyridine ligands have the NH of the triazol ring in a *syn* position to the pyridine nitrogen, coordination to a metal instead occurs with the nitrogen from the pyridyl and nitrogen group of the 1,2,3-triazole unit (see next unit), unless the $N_{triazole}$ is blocked, for example by having a CH_3 group attached to it (example CSD reference codes DUSLIO, JOCFAK, JOCFIS, ZOLPUN, WATWOF). This implies that the pyridine group needs to rotate before coordination to a metal can occur. DFT calculations show that the energy barrier, upon rotation from the optimised *syn* to the optimised *anti* geometry of ligand 8 (with R = H on L^{8}), is only 0.38 eV (36 kJ mol^{-1} or 8.7 kcal mol^{-1}), which is *ca.* three times the C-C bond rotation barrier of ethane [39], see Figure 4.

The highest occupied molecular orbitals (HOMOs) of the ligands show extended π-character, which expands over the whole ligand (Figure 5), explaining the sensitivity of the ^{1}H NMR C-H-triazole peak on the electron donating/withdrawing power of the various R substituents on the 2-[1-(4-R-phenyl)-1H-1,2,3-triazol-4-yl]pyridine ligands.

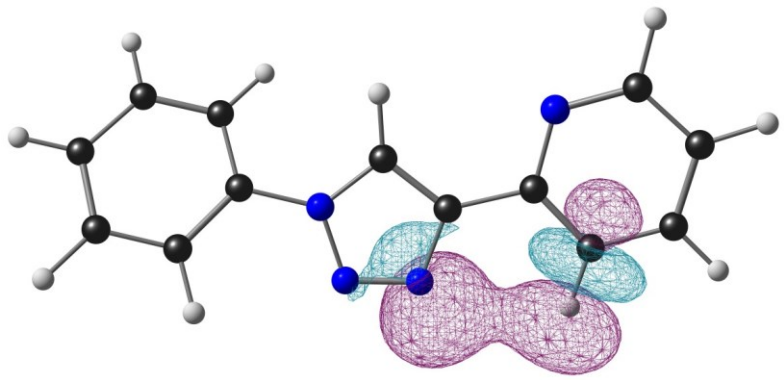

Figure 3. Optimised geometry of ligand 8 (with group R = H on L^{8}), showing the LP(N) -> BD*(C-H) NBO interaction. Colour code of atoms (online version): N (blue), O (red), Cl (green), C (black), H (white).

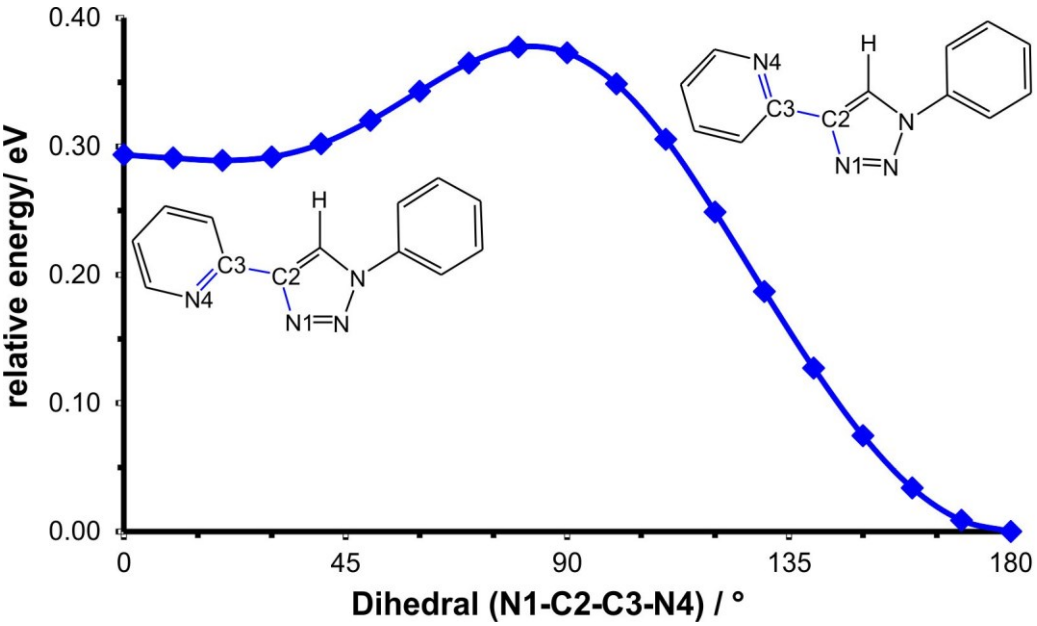

Figure 4. Potential energy surface scan along the $N1_{triazol}$-C2-C3-$N4_{pyridine}$ dihedral angle of ligand 8 (with group R = H on L^8).

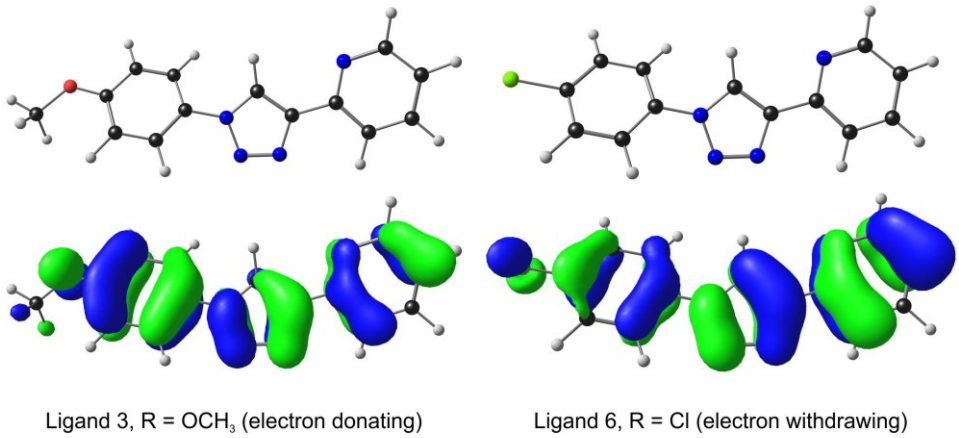

Figure 5. HOMOs of the indicated ligands (with group R = OCH_3 on L^3; group R = Cl on L^6). Colour code of atoms (online version): N (blue), O (red), Cl (green), C (black), H (white). A contour value of 30 e/nm^3 has been used to generate the orbital plots.

3.2 Characterisation of the Fe-ligand complexes

Complex formation of the bidentate (1,2,3-triazol-4-yl)pyridine ligands with iron occur with the pyridyl 1,2,3-triazole nitrogens (Scheme 2). The complexes were prepared in a 1 : 2 mole ratio of iron : ligand and were characterized by different techniques, such as FT-IR, MS, NMR, UV-Vis, melting points, electrochemistry and computational chemistry calculations. The IR spectra of the Fe compounds exhibited bands with appropriate shifts, due to complex formation. This indicates

coordination of the nitrogen from the C=N pyridine moiety, to the iron atom. The coordination mode is determined by the X-ray molecular structure analysis of a crystal of complex **3** $[Fe(L^3)_2Cl_2]$, with substituent R = OCH_3 on L^3, as a representative example of complexes **2** to **9**. The experimentally measured magnetic moments for complexes **2** – **9** are 5.26, 5.07, 5.1, 4.87, 5.10, 4.26, 4.66, 4.72 B.M. respectively, consistent with high spin S = 2 iron(II) complexes. Some iron(II) compounds containing 2-pyridyl-1,2,3-triazole ligands are reported to be low spin [40] and other high spin at room temperature, and some exhibit spin crossover properties [41]. For example, certain iron(II) complexes with ferrocene-containing triazole-pyridine ligands, *trans*-$[Fe(Fctzpy)_2(NCX)_2]\cdot CHCl_3$ (Fc-tzpy = 4-(2-pyridyl)-1H-1,2,3-triazol-1-ylferrocene, X = S (1) and X = Se (2)) exhibit spin crossover display thermal- and light-induced spin crossover properties. The crystal structure of both 1 (X = S) and 2 (X = Se) at 275 K is consistent with the iron(II) ion in the high-spin state while the crystal structure of 2 (X = Se) at the low temperature of 120 K is consistent with the iron(II) ion in the low-spin state [42].

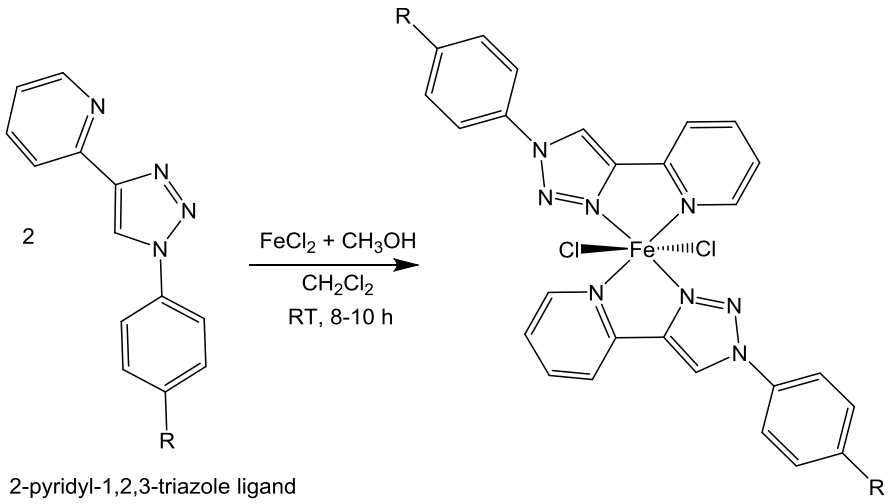

Scheme 2. Synthesis of the various eight [Fe(L^n)$_2$Cl$_2$] complexes (where n = 2 to 9) from the ligands, L_2 – L_9. Substituent R = CH_3 (L^2), OCH_3 (L^3), COOH (L^4), F (L^5), Cl (L^6), CN (L^7), H (L^8) and CF_3 (L^9).

3.2.1 X-ray structure of complex **3** $[Fe(L^3)_2Cl_2]$ with substituent R = OCH_3 on L^3

A perspective drawing of the molecular structure of complex $[Fe(L^3)_2Cl_2]$ (with substituent R = OCH_3 on L^3), including the atom numbering scheme, is shown in Figure 6. Crystallographic data is presented in Table 1, with selected bond lengths (Å) and bond angles (°) listed in Table 2. Complex **3**, $[Fe(L^3)_2Cl_2]$, crystallises in the monoclinic $P2_1/c$ space group. The iron centre in $[Fe(L^3)_2Cl_2]$ is in a distorted octahedral coordination arrangement, which includes two of the 2-(1-(4-methoxy-phenyl)-*1H*-1,2,3-triazol-4-yl) pyridine ligands, coordinated via the $N8_{triazol}$ and $N1_{pyridine}$ atoms from the two ligands L^3, to the iron centre. The iron atom lies on an inversion centre with the asymmetric unit containing the iron, a chloride and one ligand and so the iron coordination

requirement is completed by this symmetry operation. The Ni–$N1_{pyridine}$, Ni–$N8_{triazol}$ and Ni-Cl bond lengths are 2.2018(15) Å, 2.1838(16) Å and 2.4456(5) Å respectively. The iron-triazole bond length is *ca.* 0.02 Å shorter than the iron-pyridine bond length. Atoms $N8^{eq}$–Fe–$N1^{eq}$ ($N_{(pyridine)}$ 1 –Fe–$N_{(triazole)}$) lie in the equatorial plane, at an angle of 75.90(6)°. The inversion symmetry means that the $N1_{pyridine}$, $N8_{triazol}$ and Cl1 are trans to their symmetry equivalents with bond angles e.g. $N8^{eq}$–Fe–$N8i^{eq}$ of 180.0°. The N8–N9, N9–N10 and N8–C7 bond lengths of the 1,2,3-triazole ring are 1.311(2) Å, 1.354(2) Å and 1.360(2) Å respectively, and are essentially the same as the corresponding bond lengths in the free ligand (L^3), of N8–N9 1.307(4) Å, N9–N10 1.366(6) Å and N8–C7 1.362(5) Å [10]. The pyridine ring and the plane through the triazole ring are coplanar with an angle between them of 0.66°, while the plane through the substituted phenyl ring has an angle of 12.04° with the latter. A *trans* orientation of the triazole ligands in the same plane, with the $N_{pyridine}$ and $N_{triazol}$ donors *trans* to each other, has recently been found for octahedral $[Ni(L^2)_2Cl_2]$ [20], $[Zn(L^2)_2Cl_2]$ [20], $[Co(L^3)_2Cl_2]$ [43], $[Ni(L^3)_2Cl_2]$ [43] and in a related octahedral nickel complex containing two 1-(cyclohexyl)-4-(2-pyridyl)-1,2,3-triazole ligands and two *trans* bromo atoms [44]. A further example is the square planar Pd(II) complex with two 4-(2-Pyridyl)-1-phenyl-1H-1,2,3-triazole ligands [45]. However, in octahedral $[Mn(L^3)_2Cl_2]$ [43], the two chloro ligands are adopting the *cis* positions around the Mn centre.

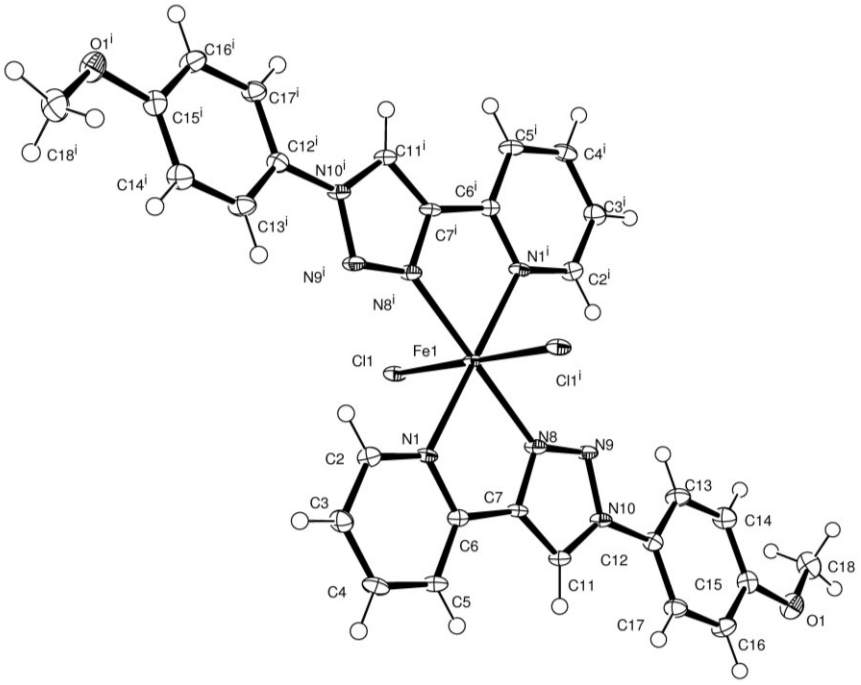

Figure 6. A perspective drawing of the molecular structure of complex $[Fe(L^3)_2Cl_2]$ (with group R = OCH_3 on ligand L^3), showing the atom numbering scheme. The asymmetric unit contains one half of the complex, with the Fe site lying on an inversion centre, with the other ligand and Cl atom being generated by inversion symmetry. Displacement ellipsoids are drawn at 50% probability level.

Several weak intermolecular hydrogen bonding and π…π interactions lead to a 3D supramolecular structure, see Figure 7. Weak intramolecular hydrogen bonding interactions, C11-H11....Cl and C17-H17.....Cl involving the chloro moieties, as well as C18-H18....N9 involving the methoxy group, are present with H…Acceptor distances for H11...Cl (2.563Å) and H17...Cl (2.867Å) which are well below the sum of the Van der Waals radii of H and Cl (3Å) [46]. The intramolecular H18....N9 distance of 2.632 Å is quite long, but still shorter than the sum of their Van der Waals radii (2.75Å), and is comparable with other published results [47,48]. The triazole $C_7N_8N_9N_{10}C_{11}$ and pyridine $N_1C_2C_3C_4C_5C_6$ rings stack in a face–to–face parallel manner, exhibiting a centroid–centroid distance of 3.566 Å and plane to centroid distance of 3.404 Å. The phenyl $C_{12}C_{13}C_{14}C_{15}C_{16}C_{17}$ and triazole $C_7N_8N_9N_{10}C_{11}$ rings of the neighboring molecules are separated by 4.116 Å, with a 3.487 Å plane to centroid distance, which is indicative of a slipped-type parallel alignment, see Figure 7. These distances are comparable to previously reported bond separations typical of π…π stacking [49]. triazole rings.

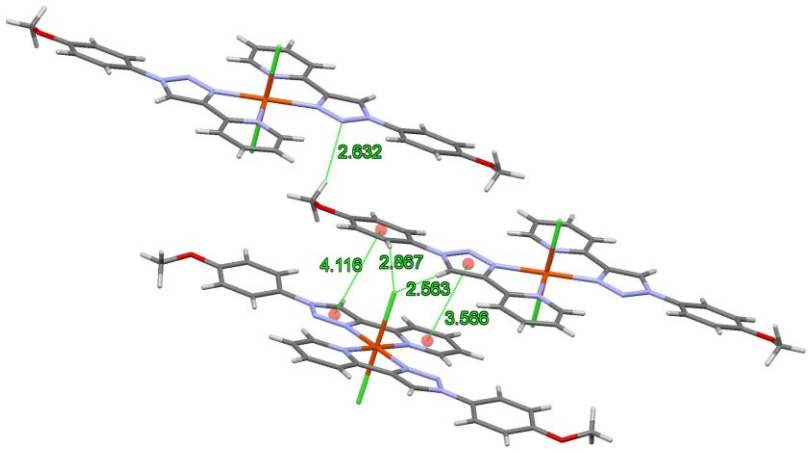

Figure 7. Partial packing of $[Fe(L^3)_2Cl_2]$, showing intermolecular hydrogen bonding interactions (C–H…Cl and C–H…N) and π…π stacking distances (Å), involving the triazole - pyridyl and phenyl - triazole rings.

Table 1. Crystallographic data for complex $[Fe(L^3)_2Cl_2]$ (with group R = OCH_3 on ligand L^3).

Empirical formula	$C_{28}H_{24}Cl_2FeN_8O_2$
M_r	631.30
Temp/K	100(2) K
Cryst. syst.	Monoclinic
Space group	$P2_1/c$
a/Å	10.3599(7)
b/Å	13.1029(8)
c/Å	10.2300(6)
α/°	90.00

β/°	96.161(7)
γ/°	90.00
V/Å^3	1380.65(15)
Z	2
R_{int}	0.0387
D_{calcd}/g cm^{-3}	1.519
Refln (all/ind/obsd)	6581/3143/2754
μ/mm^{-1}	0.783
$R1$ (obsd data: $F^2 > 2\sigma(F^2)$)[a]	0.0398
$wR2$ (all data)[a]	0.1063

Table 2. Selected bond lengths (Å) and bond angles (°) for complex [Fe(L^3)$_2$Cl$_2$] (with R = OCH$_3$).

Bond distance (Å)		**Bond angles (°)**	
C7–C11	1.375(3)	N$_{(pyridine)}$ 1 –Fe–N $_{(pyridine)}$ 1^i	180
N8–N9	1.311(2)	N $_{(triazole)}$ 1^i –Fe–N $_{(triazole)}$ 1	180
N9–N10	1.354(2)	N$_{(pyridine)}$ 1–Fe–N $_{(triazole)}$ 1^i	104.10(6)
N8–C7	1.360(2)	N$_{(pyridine)}$ 1 –Fe–N $_{(triazole)}$ 1	75.90(6)
Fe–N$_{(pyridine)}$ 1	2.2018(15)	N$_{(pyridine)}$ 1–Fe– Cl 1	89.80(4)
Fe–N$_{(triazole)}$1	2.1838(16)	N$_{(pyridine)}$ 1^i –Fe– Cl 1	90.20(4)
Fe–Cl 1	2.4456(5)	N $_{(triazole)}$ 1^i –Fe– Cl 1	90.20(4)
		N $_{(triazole)}$ 1 –Fe– Cl 1	89.80(4)
		Cl 1 ^{i} –Fe– Cl 1	180

i Symmetry transformation used to generate equivalent atoms –x+1,–y+1,–z

3.2.2 DFT study of the Fe-complexes

Five geometrical isomers, three *cis* and two *trans*, are possible for each of the eight Fe complexes of this study, containing two (1,2,3-triazol-4-yl)pyridine ligands and two chloride atoms attached to the iron centre. The five isomers for complex [Fe(L^8)$_2$Cl$_2$], with R = H on ligand L**^{8}**, are shown in Figure 8. The d^6 [Fe(L)$_2$Cl$_2$] complexes of this study are high spin complexes with a $t^4_{2g}e^2_g$ ground state [50]. This is confirmed by the experimentally measured magnetic moment of 5.07 B.M for complex 3. To confirm the spin state of S = 2, the five isomers of [Fe(L^8)$_2$Cl$_2$] were each optimized for all the possible spin states of a d^6 complex (namely S = 0, 1 or 2). The relative energies given in **Table 3** clearly show, in agreement with experiment, that [Fe(L^8)$_2$Cl$_2$] is high spin with S = 2. The two lowest energy isomers, one *cis* and one *trans*, are the isomers with the pyridine groups positioned *trans* to each other. The lowest energy isomer is the same *trans* isomer as has been obtained experimentally for complex [Fe(L^3)$_2$Cl$_2$], with R = OCH$_3$ on ligand L^3.

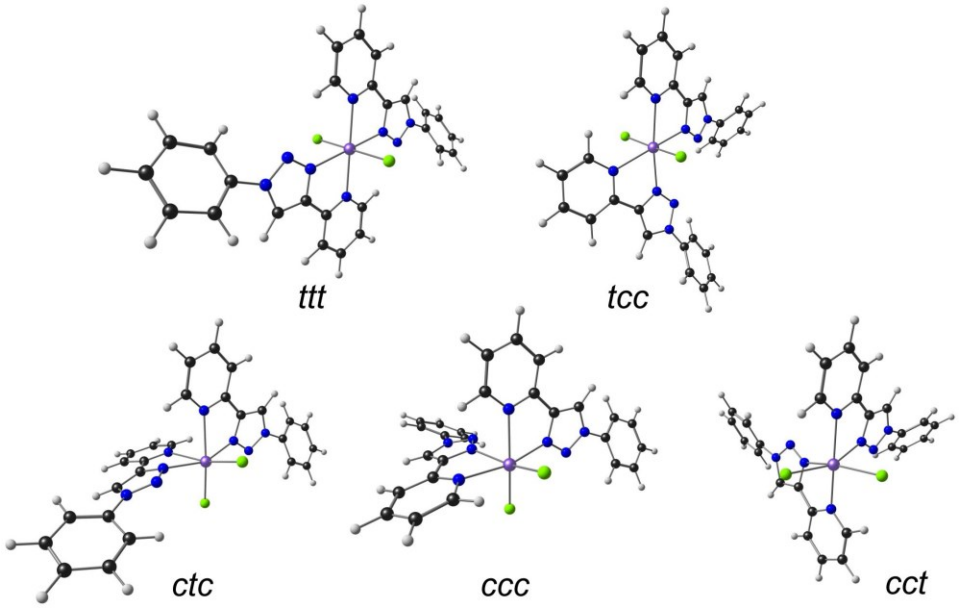

Figure 8. DFT optimized geometries for the two *trans* and three *cis* geometrical isomers possible for complex $[Fe(L^8)_2Cl_2]$ (with R = H on ligand L^8). The *trans* (*t*) and *cis* (*c*) assignment is according to the relative positions of (1) Cl, (2) $N_{triazole}$ and (3) $N_{pyridine}$. Colour code of atoms (online version): Fe (purple), Cl (green), N (blue), C (black), H (white).

Table 3. Relative energies (eV) for the different spin states and geometrical isomers of $[Fe(L^8)_2Cl_2]$.

Isomer[a]	S	Electronic energy E (eV)[b]	Gibbs energy G (eV)
ctc	0	1.11	1.35
ccc		0.88	1.12
cct		0.63	0.88
ttt		0.61	0.83
tcc		0.89	1.12
ctc	1	1.18	1.26
ccc		0.97	1.07
cct		0.78	0.88
ttt		1.95	2.09
tcc		0.91	0.98
ctc	2	0.48	0.44
ccc		0.27	0.26
cct		0.10	0.10
ttt		**0.00**	**0.00**
tcc		0.19	0.16

a See Figure 8 for the geometry of the different isomers.

b E from reference [20].

Complexes **2** to **9** of this study are d^6 Fe(II) complexes, with the ligands arranged in a distorted octahedron geometry around Fe(II). Evaluation of the frontier orbitals of the DFT optimised complex **8**, shows that the HOMO is 98% d_{xy} Fe based, see Figure 9 top. The first electron to be

removed upon oxidation of the Fe(II) complex, will thus be a Fe d_{xy} electron from the HOMO, with the formation of Fe(III). The character of the LUMO of oxidized **8** (93% d_{xy} Fe), the orbital from which the electron was removed upon oxidation (Figure 10 bottom), confirms that oxidation of **8** is iron metal based. The HOMO of oxidized **8** (Figure 10 top), however, has 58% chloride character, suggesting that the next oxidation (experimentally observed at c.a. 0.7 V *versus* Fc/Fc^{+}) involves chloride. The LUMO of the neutral complex **8** is (1,2,3-triazol-4-yl)pyridine ligand based. Reduction of **8** is therefore also (1,2,3-triazol-4-yl)pyridine ligand based. It is not expected that electron withdrawing or donating R substituents will have a large influence on the value of the $Fe^{II/III}$ redox couple, since the HOMO does not have any ligand character whatsoever, that could transpose any electron density via conjugation from the R substituent to Fe.

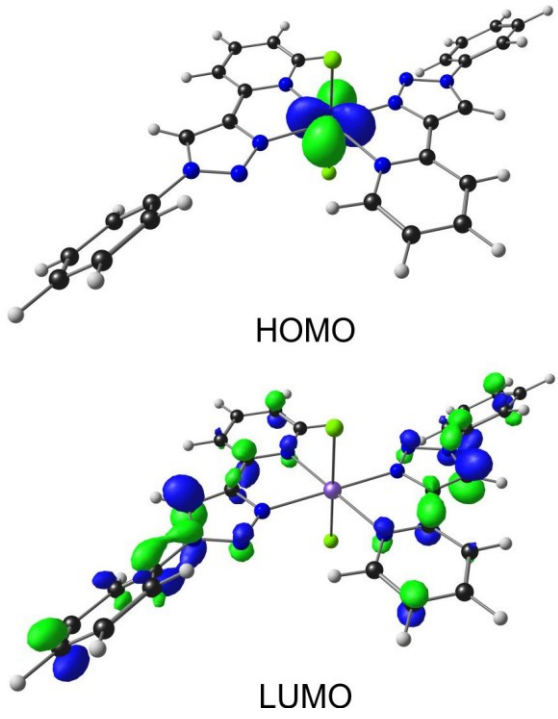

Figure 9. Frontier orbitals of complex $[Fe(L^8)_2Cl_2]$ (with R = H on ligand L^8). Colour code of atoms (online version): Fe (purple), N (blue), C (black), H (white). A contour value of 60 e/nm^3 has been used to generate the orbital plots. Colour code (online version): Fe (purple), C (grey), N (blue) and H (white).

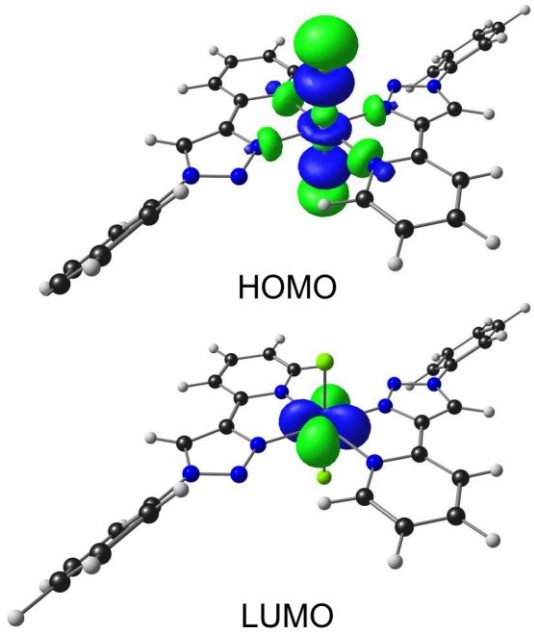

Figure 10. LUMO and HOMO of $[Fe(L^8)_2Cl_2]^+$ (with R = H on L^8). A contour value of 60 e/nm^3 has been used to generate the orbital plots. Colour code of atoms (online version): Fe (purple), N (blue), C (black), H (white).

3.2.3 Electrochemistry of the eight Fe-complexes

The cyclic voltammograms of the eight Fe(II) – (1,2,3-triazol-4-yl)pyridine complexes, **2** – **9**, all show the following electrochemical peaks: a small chemical reversible redox couple at *ca.* –0.3 V *versus* Fc/Fc^+, two or more irreversible reduction peaks below –1.5 V *versus* Fc/Fc^+, and an irreversible oxidation peak at *ca.* 0.7 V *versus* Fc/Fc^+, see Figure 11 (left). The chemical reversible redox couple at *ca.* –0.3 V *versus* Fc/Fc^+ is assigned to the $Fe^{II/III}$ redox couple, based on the character of the HOMO of these complexes, as described in the previous section. The large irreversible oxidation peak at *ca.* 0.7 V *versus* Fc/Fc^+ is assigned to the chloride oxidation, based on the character of the HOMO of the oxidised complexes (cations), as also described in the previous section. A value of c.a. 0.7 V *versus* Fc/Fc^+ for coordinated chloride oxidation, agree quantitatively with chloride oxidation, since the standard oxidation potential Cl^- is 1.34 V versus NHE, *i.e.* (1.34-0.244) V = 1.1 V *versus* SCE, or (1.1 - 0.525) V = 0.58 V *versus* Fc/Fc^+).

The first observed reduction is assigned to the reduction of the (1,2,3-triazol-4-yl)pyridine ligand, based on the character of the LUMO of the neutral complexes. A graph of the cyclic voltammograms (CVs) of the chemical reversible $Fe^{II/III}$ redox couple at *ca.* –0.3 V *versus* Fc/Fc^+, is given in Figure 11 (right). The values of the $Fe^{II/III}$ redox couple are electrochemically irreversible (meaning large oxidation and reduction peak separations) and vary over a very small potential range of *ca.* 0.05 V, for the $Fe^{II/III}$ redox couple of all eight complexes, **2** – **9**. The various R substituents (Scheme 2) on the eight different ligands (L^2 – L^9) of these complexes, therefore have virtually no

influence on the values of the $Fe^{II/III}$ redox couple for complexes **2** – **9**, as was expected from the character of the HOMOs of complexes **2** – **9**, which did not demonstrate any communication of electron density between the ligand and the Fe metal. A similar result was obtained for a series of eight *fac*-$Re(CO)_3Cl$-pyridyl-1,2,3-triazole containing substituted 2-(1-R-1H-1,2,3-triazol-4-yl)pyridine ligands where the position of the Re-based oxidation were found to be essentially unaffected by the electronic nature of the different R substituents (octyl, Bn, 4-methoxybenzyl, 4-nitrobenzyl, phenyl, ferrocenyl, 4-methoxyphenyl and nitrophenyl) [51].

The commonly used iodide/triiodide (I_3^-/I^-) redox mediator used in dye-sensitized solar cells, DSSC [52] has an average redox potential of -0.34 ± 0.02 V vs Fc/Fc^+ in acetonitrile [53]. Complexes **2** – **9** with a similar redox potential may thus qualify as alternative redox mediators. "Ultimately, the election of a determined couple as mediator will depend mainly on the electronic properties of the specific dye in a given cell" [54].

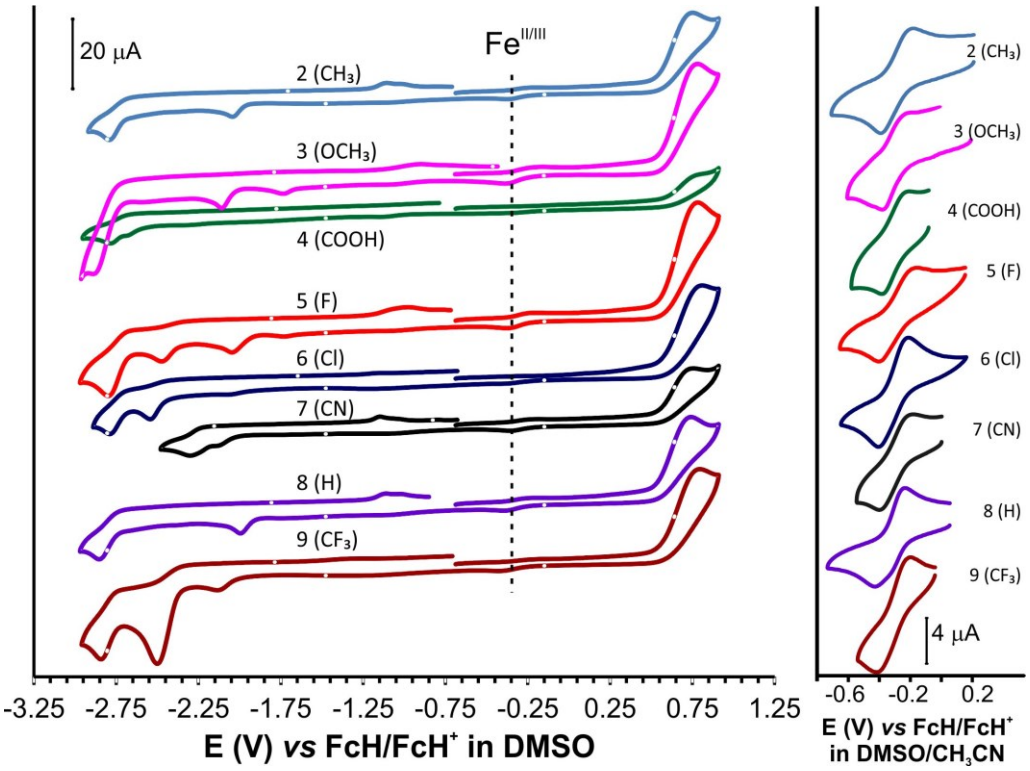

Figure 11. Cyclic voltammograms recorded at 0.100 V s^{-1}, of complexes 2 to 9: Left: Wide scans in DMSO, Right: Region of the $Fe^{II/III}$ redox couple for each complex, in DMSO : CH_3CN (1 : 3) solution. The y-axis denotes relative current. Values $E^{o'}$ (V *vs.* Fc/Fc^+) = -0.287, -0.282, -0.296, -0.281, -0.311, -0.295, -0.333 and -0.310 V, for complexes 2 to 9 respectively.

4 Summary

Eight different dichloro(bis{2-[1-(4-R-phenyl)-1H-1,2,3-triazol-4-yl-κN^3]pyridine-κN})iron(II) complexes (**2** – **9**), with substituents R = CH_3 (L^2), OCH_3 (L^3), COOH (L^4), F (L^5), Cl (L^6), CN (L^7), H (L^8) and CF_3 (L^9), have been synthesised and characterised. The single crystal structure of **3** and theoretical DFT calculations both demonstrated a distorted octahedral geometry, with the two triazole ligands coordinated to the iron centre positioned in the equatorial plane, and the two chloro atoms in the axial positions *trans* to each other. The DFT calculations further demonstrated that the d^6 $[Fe(L)_2Cl_2]$ complexes of this study is high spin complexes with a $t^4_{2g}e^2_g$ ground state. The HOMO of the d^6 Fe(II) complexes is Fe metal-based. The LUMO on the other hand, is (1,2,3-triazol-4-yl)pyridine ligand-based. The cyclic voltammograms of all eight Fe(II) metal (1,2,3-triazol-4-yl)pyridine complexes (**2** – **9**), all show a small chemical reversible redox couple at *ca*. –0.3 V *versus* Fc/Fc^+, which was assigned to the $Fe^{II/III}$ redox couple, based on the character of the HOMO of the Fe-complexes. A second irreversible oxidation peak at *ca*. 0.7 V *versus* Fc/Fc^+ was assigned to the chloride oxidation, while the first observed reduction (below –1.5 V) was assigned to the reduction of the (1,2,3-triazol-4-yl)pyridine ligand, based on the character of the LUMO of the neutral complexes. The different R substituents on the phenyl rings of complexes **2** – **9** did not in any way influence the values of the metal $Fe^{II/III}$ redox couple, which only varied over a small potential range of only 0.05 V. This ligand independency can be explained by the character of the HOMOs of complexes **2** – **9**, which did not demonstrate any communication of electron density between the ligands and the Fe metal. The HOMOs of the free ligands, however, displayed extended π-character which expands over the entire ligand, explaining the sensitivity of the ^{1}H NMR C-H-triazole peak, which is dependent on the electron donating/withdrawing power of the different R substituents on the eight 2-[1-(4-R-phenyl)-1H-1,2,3-triazol-4-yl]pyridine ligands.

Supplementary material

Optimised coordinates of the DFT calculations and crystallographic data for **3** given in the Supporting Information. Additional electrochemical graphs and data associated with this article can be found at http://dx.doi.org/10.1016/j.dib.2018.xx.xxx.

Acknowledgements

The National Mass Spectroscopy Centre at the University of Wales, Swansea is thanked for supplying the mass spectrometry data. XRD data and structures were supplied by the National

Crystallography Service at the University of Southampton. KT expresses his gratitude to the Iraqi Government for financial support to conduct the research reported in the UK and EPSRC for funding the UK National Crystallography Service. This work has received support from the South African National Research Foundation and the Central Research Fund of the University of the Free State, Bloemfontein, South Africa. The authors acknowledge High Performance Computing facility of the University of the Free State and the Centre for High Performance Computing (CHPC), South Africa, for providing computational resources to this research project.

References

[1] M.B. Smith, J. March, March's Advanced Organic Chemistry: Reactions, Mechanisms, and Structure, 5th Edition, Molecules 6 (2001) 1064-1065. DOI:10.3390/61201064
[2] M.B. Smith, Organic Synthesis Second Edition, 3.9. A Oxidation of sulfur compounds, Department of Chemistry, University of Connecticut, USA, 2002.
[3] E.J. Corey, Enantioselective Catalysis Based on Cationic Oxazaborolidines, Angew. Chem. Int. Ed. 48 (2009) 2100-2117. DOI:10.1002/anie.200805374
[4] J.D. Worley, Heterocyclic chemistry, second edition (Gilchrist, T.L.), J. Chem. Educ. 70 (1993) A89. DOI:10.1021/ed070pA89.1
[5] B. Schulzeab, U.S. Schubert, Beyond click chemistry – supramolecular interactions of 1,2,3-triazoles, Chem. Soc. Rev. 43 (2014) 2522 -2571. DOI: 10.1039/c3cs60386e.
[6] R.N. Kumar, G. Mallareddy, P. Nagender, P.S. Rao, Y. Poornachancra, P. Ranjithreddy, C.G. Kumar, B. Narsaiah, Synthesis of novel triazole functionalized pyridine derivatives as potential antimicrobial and anti-biofilm agents, IJC, 55B (11) 1361-1375. http://nopr.niscair.res.in/handle/123456789/37033
[7] H.Y.V. Ching, X. Wang, M. He, N.P. Holland, R. Guillot, C. Slim, S. Griveau, H.C. Bertrand, C. Policar, F. Bedioui, M. Fontecave, Rhenium Complexes Based on 2-Pyridyl-1,2,3-triazole Ligands: A New Class of CO2 Reduction Catalysts, Inorg. Chem. 56 (2017) 2966-2976, DOI: 10.1021/acs.inorgchem.6b03078
[8] L. Liang, D. Astruc, The copper(I)-catalyzed alkyne-azide cycloaddition (CuAAC) "click" reaction and its applications. An overview, Coord. Chem. Rev. 255 (2011) 2933– 2945. DOI: 10.1016/j.ccr.2011.06.028
[9] S. Paek, C. Baik, M. Kang, H. Kang, J. Ko, New type of ruthenium sensitizers with a triazole moiety as a bridging group, J.Organometal. Chem. 695 (2010) 821–826. DOI: 10.1016/j.jorganchem.2009.12.021
[10] K.M. Tawfiq, G.J. Miller, M.J. Al-Jeboori, P.S. Fennell, S.J. Coles, G.J. Tizzard, C. Wilson, H. Potgieter, Comparison of the structural motifs and packing arrangements of six novel derivatives and one polymorph of 2-(1-phenyl-1H-1,2,3-triazol-4-yl)pyridine, Acta Cryst. B70 (2014) 379–389. DOI:10.1107/S2052520614001152
[11] D. Kumar, V.B. Reddy, An Efficient, One-Pot, Regioselective Synthesis of 1,4-Diaryl-1*H*-1,2,3-triazoles using Click Chemistry, Synthesis (2010) 1687-1691. DOI:10.1055/s-0029-1218765
[12] F. Alonso, Y. Moglie, G. Radivoy, M. Yus, Click chemistry from organic halides, diazonium salts and anilines in water catalysed by copper nanoparticles on activated carbon, Org. & Biomol. Chem. 9 (2011) 6385-6395. DOI: 10.1039/C1OB05735A

[13] I.S. Park, M.S. Kwon, Y. Kim, J.S. Lee, J. Park, Heterogeneous copper catalyst for the cycloaddition of azides and alkynes without additives under ambient conditions, Org. Lett. 10 (2008) 497-500. DOI: 10.1021/ol702790w
[14] H. Park, Pharmaceutical Patent Analyst. 3 (2014) 491-498.
[15] M. Wolff, L. Munoz, A. François, C. Carrayon, A. Seridi, N. Saffon, C. Picard, B. Machura, E. Benoist, Tricarbonylrhenium complexes from 2-pyridyl-1,2,3-triazole ligands bearing a 4-substituted phenyl arm: a combined experimental and theoretical study, J. Chem. Soc., Dalton Trans. 42 (2013) 7019-7031. DOI:10.1039/C3DT33071K
[16] D. Schweinfurth, R. Pattacini, S. Strobel, B. Sarkar, New 1,2,3-triazole ligands through click reactions and their palladium and platinum complexes, J. Chem. Soc., Dalton Trans. (2009) 9291-9297. DOI:10.1039/B910660J
[17] J.D. Crowley, P.H. Bandeen, L.R. Hanton, A one pot multi-component CuAAC "click" approach to bidentate and tridentate pyridyl-1,2,3-triazole ligands: Synthesis, X-ray structures and copper(II) and silver(I) complexes, Polyhedron 29 (2010) 70-83. DOI:10.1016/j.poly.2009.06.010
[18] K.J. Kilpin, E.L. Gavey, C.J. McAdam, C.B. Anderson, S.J. Lind, C.C. Keep, K.C. Gordon, J.D. Crowley, Palladium(II) Complexes of Readily Functionalized Bidentate 2-Pyridyl-1,2,3-triazole "Click" Ligands: A Synthetic, Structural, Spectroscopic, and Computational Study, Inorg. Chem. 50 (2011) 6334-6346. DOI:10.1021/ic200789b
[19] J.P. Byrne, J.A. Kitchen, O. Kotova, V. Leigh, A.P. Bell, J.J. Boland, M. Albrecht, Th. Gunnlaugsson, Synthesis, structural, photophysical and electrochemical studies of various d-metal complexes of btp [2,6-bis(1,2,3-triazol-4-yl)pyridine] ligands that give rise to the formation of metallo-supramolecular gels, Dalton Trans. 43 (2014) 196-209. DOI:10.1039/C3DT52309H
[20] J. Conradie, M.M. Conradie, K.M. Tawfiq, M.J. Al-Jeboori, S.J. Coles, C. Wilson, J.H. Potgieter, Novel dichloro(bis{2-[1-(4-methylphenyl)-1H-1,2,3-triazol-4-yl-κN^3]pyridine-κN})metal(II) coordination compounds of seven transition metals (Mn, Fe, Co, Ni, Cu, Zn and Cd), Polyhedron 151 (2018) , 243-254. DOI: 10.1016/j.poly.2018.03.026
[21] G.A. Bain, J.F. Berry, Diamagnetic Corrections and Pascal's Constants, J. Chem. Educ. 85 (2008) 532-536. DOI:10.1021/ed085p532
[22] S.J. Coles and P.A. Gale, Changing and challenging times for service crystallography, Chem. Sci. 3 (2012) 683-689. DOI: 10.1039/C2SC00955B
[23] O.V. Dolomanov, L.J. Bourhis, R.J. Gildea, J.A.K. Howard, H. Puschmann, OLEX2: A Complete Structure Solution, Refinement and Analysis Program, J. Appl. Cryst. 42 (2009) 339-341. DOI: 10.1107/S0021889808042726
[24] G.M. Sheldrick, A short history of SHELX, Acta Cryst. Sect. A. 64 (2008) 112-122. DOI:10.1107/S0108767307043930
[25] P.T. Kissinger, W.R. Heineman, Cyclic Voltammetry, J. Chem. Ed. 60 (1983) 702-706. DOI:10.1021/ed060p702
[26] D.T Sawyer, J.L Roberts (Jr), Experimental Electrochemistry for Chemists, Wiley, New York, 1974, p. 54.
[27] D.H. Evans, K.M. O'Connell, R.A. Peterson, M.J. Kelly, Cyclic Voltammetry, J. Chem. Ed. 60 (1983) 290-292. DOI:10.1021/ed060p290
[28] G.A. Mabbott, An introduction to Cyclic Voltammetry, J. Chem. Ed. 60 (1983) 697-702. DOI:10.1021/ed060p697
[29] G. Gritzner, J. Kuta, Recommendations on reporting electrode potentials in non-aqueous solvents, Pure and Applied Chemistry 56 (1984) 461-466. DOI:10.1351/pac198456040461.
[30] H.-M. Koepp, H. Wendt, H. Strehlow, Comparison of the Potential Series in Different Solvents, Zeitschrift für Elektrochemie 64 (1960) 483-491. DOI:10.1002/bbpc.19600640406
[31] M.J. Frisch, G.W. Trucks, H.B. Schlegel, G.E. Scuseria, M.A. Robb, J.R. Cheeseman, G. Scalmani, V. Barone, B. Mennucci, G.A. Petersson, H. Nakatsuji, M. Caricato, X. Li, H.P. Hratchian, A.F. Izmaylov, J. Bloino, G. Zheng, J.L. Sonnenberg, M. Hada, M. Ehara, K. Toyota, R. Fukuda, J. Hasegawa, M. Ishida, T. Nakajima, Y. Honda, O. Kitao, H. Nakai, T. Vreven, J.A. Montgomery (Jr.), J.E. Peralta, F. Ogliaro, M. Bearpark, J.J. Heyd, E. Brothers, K.N. Kudin, V.N. Staroverov, R. Kobayashi, J. Normand, K. Raghavachari, A. Rendell, J.C. Burant, S.S. Iyengar, J.

Tomasi, M. Cossi, N. Rega, J.M. Millam, M. Klene, J.E. Knox, J.B. Cross, V. Bakken, C. Adamo, J. Jaramillo, R. Gomperts, R.E. Stratmann, O. Yazyev, A.J. Austin, R. Cammi, C. Pomelli, J.W. Ochterski, R.L. Martin, K. Morokuma, V.G. Zakrzewski, G.A. Voth, P. Salvador, J.J. Dannenberg, S. Dapprich, A.D. Daniels, Ö. Farkas, J.B. Foresman, J.V. Ortiz, J. Cioslowski, D.J. Fox, Gaussian 09, Revision D.01, Gaussian, Inc., Wallingford, CT, 2009.
[32] J.P. Foster, F. Weinhold, Natural hybrid orbitals, J. Am. Chem. Soc. 102 (1980) 7211-7218. DOI:10.1021/ja00544a007/
[33] A.E. Reed, F. Weinhold, Natural localized molecular orbitals, J. Phys. Chem. 83 (1985) 1736-1740. DOI:10.1063/1.449360.
[34] A.E. Reed, R.B. Weinstock, F. Weinhold, Natural population analysis, J. Chem. Phys. 83 (1985) 735-746. DOI:10.1063/1.449486.
[35] A.E. Reed, L.A. Curtiss, F. Weinhold, Intermolecular interactions from a natural bond orbital, donor-acceptor viewpoint, Chem. Rev. 88 (1988) 899-926. DOI:10.1021/cr00088a005.
[36] E.D. Glendening, J.K. Badenhoop, A.E. Reed, J.E. Carpenter, J.A. Bohmann, C.M. Morales, C.R. Landis, F. Weinhold, NBO 3.1, Theoretical Chemistry Institute, University of Wisconsin, Madison, WI, 2001.
[37] D. Schweinfurth, S. Strobel, B. Sarkar, Expanding the scope of 'Click' derived 1,2,3-triazole ligands: New palladium and platinum complexes, Inorg. Chim. Acta. 374 (2011) 253-260. DOI:10.1016/j.ica.2011.02.085
[38] Cambridge Structural Database (CSD), Version 5.38, May 2017 update, Cambridge, UK, 2017.
[39] S. Liu, Origin and Nature of Bond Rotation Barriers: A Unified View, J. Phys. Chem. A 117 (2013) 962−965. DOI:10.1021/jp312521z
[40] S.K. Vellas, J.E.M. Lewis, M. Shankar, A. Sagatova, J.D.A. Tyndall, B.C. Monk, C.M. Fitchett, L.R. Hanton, J.D. Crowley, [Fe2L3]4+ Cylinders Derived from Bis(bidentate) 2-Pyridyl-1,2,3-triazole "Click" Ligands: Synthesis, Structures and Exploration of Biological Activity, Molecules 18 (2013) 6383-6407. DOI:10.3390/molecules18066383
[41] R.W. Hogue, R.G. Miller, N.G. White, H.L.C. Feltham, G.N.L. Jameson, S. Brooker, Hysteretic spin crossover in iron(II) complexes of a new pyridine–triazole–pyrazine ligand is tuned by choice of NCE co-ligand, Chem. Commun., 2014, 50, 1435-1437. DOI: 10.1039/C3CC43922D
[42] T. Romero-Morcillo, F.J. Valverde-Muñoz, L. Piñeiro-López, M.C Muñoz, T. Romero, P. Molinac, J.A. Rea, Spin crossover in iron(II) complexes with ferrocene-bearing triazole-pyridine ligands, Dalton Trans. 44 (2015) 18911-18918. DOI: 10.1039/c5dt03084f
[43] J. Conradie, M.M. Conradie, K.M. Tawfiq, M.J. Al-Jeboori, S.J. Coles, J.H. Potgieter, Synthesis, characterisation, experimental and electronic structure of novel Dichloro(bis{2-[1-(4-methoxyphenyl)-1H-1,2,3-triazol-4-yl-kN3]pyridine-kN})metal(II) compounds, metal = Mn, Co and Ni, J. Mol. Struct. 1161C (2018) 89-99, DOI: 10.1016/j.molstruc.2018.02.036.
[44] D. Schweinfurth, C.Y. Su, S.C. Wei, P. Braunsteind, B. Sarkar, Nickel complexes with "click"-derived pyridyl-triazole ligands: weak intermolecular interactions and catalytic ethylene oligomerisation, Dalton Trans. 41 (2012) 12984-12990. DOI:10.1039/C2DT31805A
[45] (a) A. Dogan, B. Sarkar, A. Klein, F. Lissner, T. Schleid, J. Fiedler, S. Zális, V.K. Jain, W. Kaim, Complex reduction chemistry of (abpy)$PtCl_2$, abpy = 2,2'-azobispyridine: formation of cyclic $[(micro,eta_2:eta_1\text{-abpy})PtCl]_2^{(2+)}$ with a new coordination mode for abpy and a near-infrared ligand-to-ligand intervalence charge transfer absorption of the one-electron reduced state., Inorg. Chem. 43 (2004) 5973-5980; DOI:10.1021/ic049941t
(b) K.J. Kilpin, J.D. Crowley, Palladium(II) and platinum(II) complexes of bidentate 2-pyridyl-1,2,3-triazole "click" ligands: Synthesis, properties and X-ray structures, Polyhedron 29 (2010) 3111-3117. DOI:10.1016/j.poly.2010.08.021
[46] C.B. Aakeröy, T.A. Evans, K.R. Seddon, I. Pálinkó, The C–H···Cl hydrogen bond: does it exist, New J. Chem. 23 (1999) 145-152. DOI:10.1039/A809309A
[47] D. Urankar, A. Pevec, I. Turel, J.G. Košmrlj, Pyridyl Conjugated 1,2,3-Triazole is a Versatile Coordination Ability Ligand Enabling Supramolecular Associations, Cryst. Growth Des. 10 (2010) 4920-4927. DOI:10.1021/cg100993k

[48] (a) M. Mazik, D. Bläser, R. Boese, The potential of CH···N interactions in determining the crystal structures of novel 3,4-disubstituted-5-pyridinyl-isoxazoles, Tetrahedron Lett. 41 (2000) 5827-5831; DOI:10.1016/S0040-4039(00)00906-0
(b) M. Mazik, D. Bläser, R. Boese, Intermolecular CH····N/CH····O hydrogen bonds in the crystal structures of α, β-unsaturated ketones carrying a terminal pyridine subunit, Tetrahedron, 57 (2001) 5791-5797. DOI:10.1016/S0040-4020(01)00520-8
[49] (a) Y. Yang, P. Du, J. Yang, W.Q. Kan, J.F. Ma, A series of Cu(II) and Cd(II) coordination polymers constructed by 3,5-dinitrosalicylic acid and flexible bis(triazole) ligands containing different spacers, Cryst. Eng. Commun. 15 (2013) 4357-4371; DOI:10.1039/C3CE00034F
(b) C. Janiak, A critical account on π–π stacking in metal complexes with aromatic nitrogen-containing ligands, J. Chem. Soc., Dalton Trans. (2000) 3885-3896. DOI:10.1039/B003010O
[50] G. Sowjanya, N.C.G. Reddy, S.L. Reddy, B.J. Reddy, R.L. Frost, Electron paramagnetic resonance and optical absorption spectral studies on covellite mineral, Spectrochim. Acta Part A 71 (2008) 751-754. DOI:10.1016/j.saa.2007.12.053
[51] T.Y. Kim, A.B.S. Elliott, K.J. Shaffer, C.J. McAdam, K.C. Gordon, J.D. Crowley, Rhenium(I) complexes of readily functionalized bidentate pyridyl-1,2,3-triazole "click" ligands: A systematic synthetic, spectroscopic and computational study, Polyhedron 52 (2013) 1391-1398. DOI: 10.1016/j.poly.2012.05.003
[52] G. Boschloo, A. Hagfeldt, Characteristics of the Iodide/Triiodide Redox Mediator in Dye-Sensitized Solar Cells, Acc. Chem. Res. 42 (2009) 1819–1826. DOI:10.1021/ar900138m
[53] X.Wang, D.M. Stanbury, The Oxidation of Iodide by a Series of Fe(III) Complexes in Acetonitrile, Inorg. Chem. 45 (2006) 3415–3423. DOI:10.1021/ic052022y
[54] F. Gajardo, B. Loeb, Spectroscopic and electrochemical properties of a series of substituted polypyridine Co(II)/Co(III) couples and their potentiality as mediators for solar cells, J. Chilean Chem. Soc. 56:2 (2011) 697-701. DOI:10.4067/S0717-97072011000200016